Wake-induced instabilities of parallel circular cylinders with tandem and staggered arrangements

Haruki Fukushima[1]; Tomomi Yagi, Ph.D.[2]; Takuya Shimoda[3]; Kyohei Noguchi, Ph.D.[4]

[1]Graduate Student, Dept. of Civil and Earth Resources Eng., Kyoto Univ., Kyoto daigaku-katsura, Nishikyo-ku, Kyoto, 615-8540, Japan (Corresponding author).
E-mail: fukushima.haruki.73c@kyoto-u.jp

[2]Professor, Dept. of Civil and Earth Resources Eng., Kyoto Univ., Kyoto daigaku-katsura, Nishikyo-ku, Kyoto, 615-8540, Japan.
E-mail: yagi.tomomi.7a@kyoto-u.ac.jp

[3]Former Graduate Student, Dept. of Civil and Earth Resources Eng., Kyoto Univ., Kyoto daigaku-katsura, Nishikyo-ku, Kyoto, 615-8540, Japan.
E-mail: takuya0310st@yahoo.co.jp

[4]Assistant Professor, Dept. of Civil and Earth Resources Eng., Kyoto Univ., Kyoto daigaku-katsura, Nishikyo-ku, Kyoto, 615-8540, Japan.
E-mail: noguchi.kyohei.7z@kyoto-u.ac.jp

Abstract

When two circular cylinders are closely arranged in parallel, the downstream cylinder frequently exhibits wake-induced vibrations (WIVs). This study investigates the classifications of WIVs in various arrangements of cylinders by considering the generation mechanisms of WIVs through a series of wind tunnel tests. The generation mechanisms are defined through flutter and time-history analyses using the quasi-steady theory. Finally, this study suggests a classification map of the arrangements with four types of generation mechanisms: vertical flutter, anti-phase coupled flutter, in-phase coupled flutter (quasi-steady applicable), and in-phase coupled flutter (quasi-steady inapplicable). Vertical flutter occurs in closely staggered cylinders and tandem cylinders with a horizontal center distance measuring 2.5–9.5 times the cylinder diameter. A key parameter for distinguishing coupled flutter is the contribution of the aerodynamic coupling terms. Furthermore, for closely staggered cylinders, two types of vibrations occur, depending on the reduced wind velocity. The arrangement of the two cylinders is slightly changed because of the static displacement of the downstream cylinder depending on the wind velocity, resulting in a change in the generation mechanism. The results pertaining to the generation mechanisms effectively explain the WIV responses of the two cylinders in various arrangements.

Keywords Wake-induced vibration; Parallel stay-cable; Wake galloping; Wake-induced flutter; Flutter derivative; Quasi-steady theory

1. Introduction

When two circular cylinders are closely arranged in parallel, such as transmission wires and cables in cable-stayed long-span bridges, wake-induced vibrations (WIVs) frequently appear in the downstream cylinder owing to the wake of the upstream cylinder. Many WIV phenomena have been observed in real bridges (Yoshimura et al., 1995; Fujino et al., 2012; Hua et al., 2019). Several wind tunnel tests and numerical analyses have been conducted to determine the characteristics of WIVs in the subcritical Reynolds number (*Re*) range.

In the literature, wake galloping (WG) and wake-induced flutter (WIF) were introduced to classify WIVs by considering vibration responses. WG is a vertical predominant vibration that occurs when two cylinders are placed in tandem at a close distance of $<6D$ (Miyata et al., 2000) or $<8.5D$ (Brika and Lanevile, 1999), where D is the cylinder diameter. WIF is a two-degree-of-freedom (2DOF) coupled vibration in the vertical and horizontal directions, and the trajectory of the downstream cylinder is often elliptical. WIF appears when two cylinders are installed in a staggered arrangement at a large distance of $8D$–$11D$ (Miyata et al., 2000) or more (Cooper and Wardlaw, 1971).

Over the past half-century, many studies have been conducted on WIVs, particularly in the subcritical *Re* region. Cooper and Wardlaw (1971) investigated the aerodynamic instabilities of parallel bundled elastic power conductors and discovered that unsteady aerodynamic forces on a downstream structure in a wake result in a coupled 2DOF instability. Simpson (1971a, 1971b), Price (1975), and Simpson and Flower (1977) employed quasi-steady aerodynamic forces to explain the coupled 2DOF instabilities of two cylinders. The term "WIF" was established based on these studies pertaining to 2DOF instabilities. In addition, Zdravkovich and Pridden (1977) and Shiraishi et al. (1986) focused on unsteady aerodynamic forces and suggested that WG is excited by switching between the gap flow and outer accelerated flow. Ruscheweyh (1983) reported interference galloping, which is caused by the flow separated from the upstream cylinder. Furthermore, Assi et al. (2010) focused on unsteady aerodynamic forces and discovered that WG is affected by unsteady vortex structure interactions between the downstream body and the wake of an upstream cylinder. Moreover, Assi et al. (2013) reported that wake stiffness affects WIVs, in addition to unsteady vortex structures in the gap. Alam and Kim (2009), Kim et al. (2009), Qin et al. (2019), and Zhang et al. (2021) conducted free vibration tests on two-tandem or staggered elastically mounted cylinders. They concluded that the WIV amplitude of the downstream cylinder is much larger than that of the upstream cylinder when the two cylinders are arranged at a distance of $\geq 3D$ (Kim et al., 2009) or $\geq 2.5D$ (Qin et al., 2019), and the vibrations appear significant for the downstream cylinder in most situations. Therefore, many experiments have been conducted with the upstream cylinder fixed to consider WIVs.

Quasi-steady and unsteady aerodynamic forces were introduced to explain the characteristics of WIVs. When the distance between two cylinders is 10–20*D*, WIVs can be described using the quasi-steady theory (Cooper and Wardlaw, 1971; Simpson, 1971a; Price, 1975). Meanwhile, because aerodynamic interference dominates, the quasi-steady theory cannot clearly describe WIVs well when two cylinders are closely arranged (Shiraishi et al., 1984; Knisely and Kawagoe, 1990). Shiraishi et al. (1986) and Matsumoto et al. (1990) reported that WIVs can be explained by considering the unsteady and quasi-steady aerodynamic forces together because the unsteadiness of the wake is promoted by the sudden decrease in pressure on the inward surface of a downstream cylinder. The authors concluded that WIVs can be explained using an unsteady aerodynamic method instead of a quasi-steady theory when two cylinders are placed close to each other. Deng et al. (2019) indicated that quasi-steady and unsteady aerodynamic forces reflect the characteristics of WIVs of staggered cylinders with a distance of 5*D* and that a negative aerodynamic stiffness might be a key factor in evoking WIVs.

Although some studies have focused on *Re* (Carmo et al., 2011; Mysa et al. 2015), natural frequency (Qin et al., 2018), and diameter difference between two cylinders (Qin et al., 2017), most studies, as mentioned in the above paragraphs, have suggested that the arrangement of the two cylinders is an important factor affecting the characteristics of WIVs. Therefore, many researchers have focused on the dependence of WIVs on the arrangement of two cylinders. For instance, the flow pattern around the fixed cylinders in each arrangement was investigated by Sumner (2010) and Zhou and Alam (2016), and classified into several types by Zdravkovich (1977, 1987), Igarashi (1981), Sumner et al. (2000), and Alam and Meyer (2013). However, although these studies facilitated the understanding of the flow structure around parallel cylinders, the dependence of aerodynamics on arrangement was not sufficiently considered. The immediate mechanisms of vibrations were also not discussed. Yagi et al. (2015) distinguished WIVs into 1DOF flutter and 2DOF coupled flutter based on their generation mechanisms, which were evaluated from the flutter derivatives (unsteady aerodynamic force coefficients) of a downstream cylinder. Moreover, the boundaries between the vibrations of two parallel cylinders with different mechanisms were unclear.

In this study, wind tunnel tests, flutter analyses, and response analyses were conducted to quantitatively classify the WIV properties for each arrangement of two parallel circular cylinders in the subcritical *Re* region. Based on the results, a classification map is proposed in terms of the generation mechanisms of WIVs for each arrangement. In addition, to further understand the characteristics of WIVs, this paper discusses the dependency of vibration mechanisms on reduced wind velocity for closely staggered cylinders.

2. Setup of wind tunnel tests

In this study, a series of wind tunnel tests were conducted to classify WIVs in terms of unsteady aerodynamic characteristics. Initially, spring-supported free vibration tests were performed to obtain the vibration response of a downstream circular cylinder in each arrangement of the two cylinders. Subsequently, based on the results of the free vibration tests, unsteady aerodynamic force measurements were performed to identify the vibration mechanisms. Then, aerostatic force measurements were conducted to discuss the generation mechanisms of WIVs based on the quasi-steady theory.

A room-circuit Eiffel-type wind tunnel at Kyoto University was used in the experiments conducted in this study. The height and width of the working section of the wind tunnel were 1.8 and 1.0 m, respectively, and its maximum wind velocity was U = 30 m/s. Near the model installation location, the turbulence intensity of the mainstream was <0.3% at 10 m/s.

Two circular cylinder models were installed in parallel in the wind tunnel, as shown in Fig. 1(a), which were made of aluminum with a diameter D of 50 mm. The lengths L of the upstream and downstream cylinders were 935 and 900 mm, respectively. The downstream cylinder, which was affected by the upstream cylinder fixed on the wind tunnel surface, was investigated based on the vibration responses and aerodynamic forces acting on the downstream cylinder.

Fig. 2 presents a definition of the arrangement of the two cylinders in the spring-supported tests. Here, X and Y represent the horizontal and vertical distances between the two cylinders at the initial condition (U = 0 m/s), respectively. However, the position of the downstream cylinder may change under the wind-on condition owing to the static displacement. The time-averaged equilibrium positions of the two cylinders are defined as W and S under the wind-on condition (U > 0 m/s). The horizontal and vertical displacements of the downstream cylinder from the equilibrium position (W and S) are defined by ξ and η, respectively. In addition, X, W, and ξ denote the downstream-side positive displacements, whereas Y, S, and η denote the downward-side positive displacements.

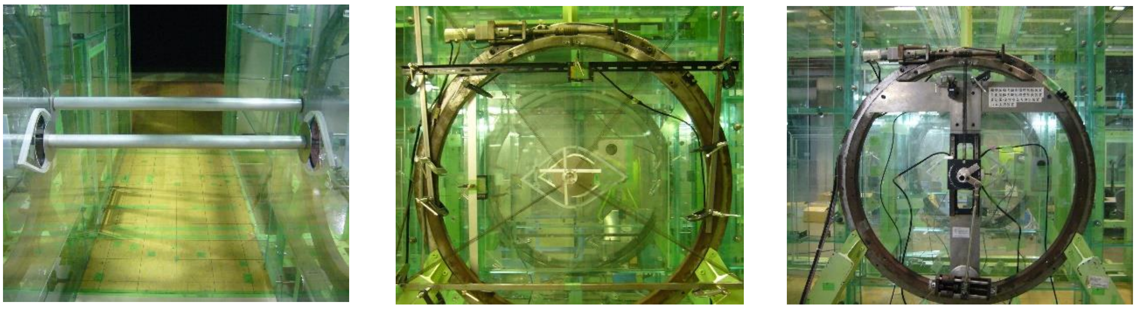

(a) (b) (c)

Fig. 1 Experimental setup: (a) parallel circular cylinders, (b) spring-supported free vibration test, and (c) forced vibration test

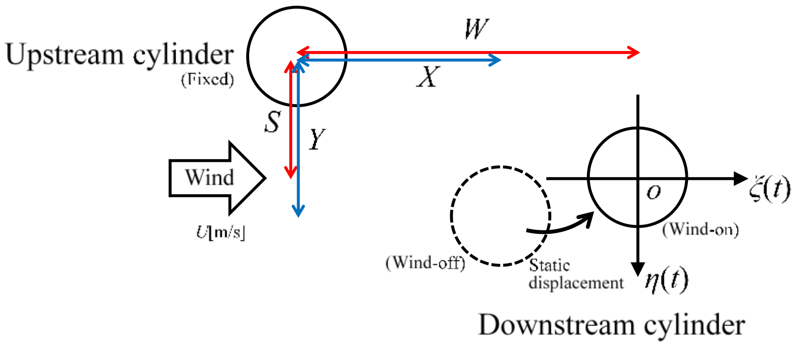

Fig. 2 Definitions of the arrangement of two cylinders and coordinate axes

2.1 Spring-supported free vibration test

The downstream cylinder was supported by four identical coil springs in an X shape at each end of the cylinder, as shown in Fig. 1(b), to realize the 2DOF system for the cylinder and simultaneously vibrate in the vertical and horizontal directions. To comprehensively investigate the WIV characteristics, X/D = 2.5–11 and Y/D = 0.0–4.0 were considered in the arrangements of the two cylinders, based on a previous study (Miyata et al., 2000). Vibration responses were measured using four laser displacement sensors (IL-300, Keyence, Japan). Two out of the four laser displacement meters were installed at one end of the cylinder, one of which was to measure the vertical displacement of the cylinder and the other the horizontal displacement. The focus of these laser displacement meters was placed on elongated targets attached to the shaft of the cylinder. One target was installed horizontally for a vertical displacement, and the other was installed vertically for a horizontal displacement. Similarly, the other two laser displacement meters and targets were installed at the opposite end. The displacements of the cylinder obtained by the laser displacement meters were recorded on a computer using a data logger (GL7000, Graphtec, Japan) with a sampling frequency of 1 kHz. The mean value of the vertical displacements obtained at both ends was used as the actual vertical displacement of the cylinder. This was also applied to the horizontal displacement. The wind velocity was U = 0–12 m/s at intervals of <3 m/s. The structural parameters of the downstream cylinder are listed in Table 1. In the table, the values with subscripts η and ξ indicate the characteristics under vertical and horizontal vibrations, respectively. The structural parameters of the ξ- and η-directions (x- and y-directions) were set to almost the same values. The logarithmic decrement in the structural damping δ and Scruton number Sc, as defined in Eq. (1), were set to the smallest possible values to easily obtain the vibration responses and focus on the aerodynamic characteristics.

$$Sc = \frac{2m\delta}{\rho D^2}, \tag{1}$$

where m is the equivalent mass per unit length [kg/m], ρ is the air density [kg/m^3], and D is the diameter of the cylinder [m].

Table 1 Structural specifications for the spring-supported free vibration tests

Cable diameter D [m]	Cable length L [m]	Equiv. mass m [kg/m]		Natural freq. f [Hz]		Log. decrement δ [-]		Scruton number Sc [-]	
		m_ξ [kg/m]	m_η [kg/m]	f_ξ [Hz]	f_η [Hz]	δ_ξ	δ_η	Sc_ξ	Sc_η
0.0500	0.900	1.38	1.33	1.37	1.42	0.0054	0.0059	5.1	5.4

2.2 Unsteady aerodynamic force measurement

In general, self-excited forces acting on a downstream cylinder indicate strong nonlinearity based on their formulations, amplitude dependencies, and multiple frequency components, among other factors. However, in this study, the characteristics of 2DOF instabilities at a downstream cylinder can be explained through the following postulations regarding unsteady aerodynamic forces, according to a previous study (Yagi et al., 2015):

1) Only the natural frequency component of the self-excited forces (*Drag* and *Lift*) is considered and obtained under the vertical or horizontal 1DOF harmonic oscillation at a natural frequency.
2) The self-excited forces (*Drag* and *Lift*) can be linearly formulated using Eqs. (2) and (3), respectively, using eight flutter derivatives (H_i, P_i, i = 1 and 4–6) (Scanlan and Tomko, 1971; Sarkar, 1994).

$$Drag = \frac{1}{2}\rho DU^2\left(kP_1^*\frac{\dot{\eta}}{U} + k^2P_4^*\frac{\eta}{D/2} + kP_5^*\frac{\dot{\xi}}{U} + k^2P_6^*\frac{\xi}{D/2}\right), \text{ and} \tag{2}$$

$$Lift = \frac{1}{2}\rho DU^2\left(kH_1^*\frac{\dot{\eta}}{U} + k^2H_4^*\frac{\eta}{D/2} + kH_5^*\frac{\dot{\xi}}{U} + k^2H_6^*\frac{\xi}{D/2}\right), \tag{3}$$

where *Drag* is the drag force per unit length [N/m] (downstream-side positive), *Lift* is the lift force per unit length [N/m] (downward-side positive), k is the reduced frequency (= $0.5D\omega/U$), ω is the circular frequency (= $2\pi f$), and U is the wind velocity [m/s].

3) The self-excited forces during the 2DOF coupling vibrations can be expressed by superimposing the vertical 1DOF unsteady aerodynamic forces on the horizontal forces with certain phase angles.

From the postulations above, {H_1*, H_4*, P_1*, and P_4*} and {H_5*, H_6*, P_5*, and P_6*} can be calculated using *Drag* and *Lift* obtained through the vertical and horizontal 1DOF harmonic oscillations, respectively.

As mentioned in Section 1, WIF has been investigated using the quasi-steady theory, and WG can be explained by H_1* as the vertical vibration. Considering these previous findings, Yagi et al. (2015) succeeded to explain various 2DOF WIVs through flutter analyses using Eqs. (2) and (3).

Furthermore, as shown in Fig. 1(c), 1DOF forced vibration tests were conducted to measure the unsteady aerodynamic forces acting on the downstream cylinder at each of the equilibrium positions obtained from the spring-supported free vibration tests. Using a motor (SD-400-11A, Shimpo Industrial, Japan), the downstream cylinder was oscillated with a vertical or horizontal 1DOF simple harmonic motion to measure the unsteady drag and lift forces by two load cells (LMC-3501-20N, Nissho Electric Works, Japan) equipped at both ends of the downstream cylinder. The drag and lift forces obtained were amplified by an amplifier (MCF-8A, Kyowa Electronic Instruments, Japan). Then, along with the displacement of the cylinder obtained using the same laser displacement meter as the spring-supported free vibration tests, they were recorded on a computer through a data logger (GL7000, Graphtec, Japan) with a sampling frequency of 1 kHz. The flutter derivatives were calculated using Eqs. (2) and (3) based on the amplitudes of the forced vibration frequency components of the unsteady aerodynamic forces and their phase lag from the displacement. These amplitudes and phase lags were evaluated using the ensemble-averaged periodic waves of the unsteady aerodynamic forces for 3 min.

The forced vibration frequency was set to f = 1.35 Hz, which corresponded to that of the spring-supported free vibration tests. The wind velocity was U = 12 m/s; hence, Re = 4.1×10^4 and the reduced wind velocity was U/fD = 177.8. The double amplitude of the vibration was $2A_\xi$ = 10, 40, and 80 mm ($2A_\xi/D$ = 0.2, 0.8, and 1.6) in the horizontal direction and $2A_\eta$ =10, 60, and 120 mm ($2A_\eta/D$ = 0.2, 1.2, and 2.4) in the vertical direction.

2.3 Aerostatic force measurement

Aerostatic force coefficients are required in the investigation of the generation mechanisms of WIVs using the quasi-steady theory. However, a sufficiently large number of arrangements of two cylinders must be considered to obtain aerostatic forces. Therefore, in this study, to efficiently measure the aerostatic forces acting on the downstream cylinder, 1DOF horizontal forced vibration tests were conducted using the same equipment described in Section 2.2, assuming that an extremely low vibration frequency can reproduce the static conditions. The double amplitude was $2A_\xi = 120$ mm ($2A_\xi/D = 2.4$), and the vibration frequency was $f_\xi = 0.027$ Hz. The time-averaged drag force F_D [N/m] (downstream-side positive in the wind direction) and lift force F_L [N/m] (downward-side positive) were measured for each arrangement to calculate the drag and lift coefficients C_D and C_L, respectively, as expressed in Eq. (4):

$$C_D = \frac{F_D}{1/2\,\rho U^2 D} \text{ and } C_L = \frac{F_L}{1/2\,\rho U^2 D}\,. \qquad (4)$$

3. Characteristics of the WIVs of downstream cylinders

This section describes the process of creating a classification map based on the generation mechanisms of WIVs for each arrangement of the two cylinders. First, the vibration responses of a downstream cylinder for each arrangement of the two cylinders were analyzed using spring-supported free vibration tests. Second, flutter analyses were conducted to classify the generation mechanisms using flutter derivatives calculated from the unsteady aerodynamic forces. Third, time-history response analyses were conducted to discuss the generation mechanisms based on the applicability of quasi-steady aerodynamic forces. Finally, by combining these results, a classification map of WIVs based on the generation mechanisms is suggested.

3.1 Spring-supported free vibration response of the downstream cylinder

Fig. 3 shows the trajectories obtained from the 2DOF spring-supported free vibration tests at a wind velocity of U = 12 m/s (U/fD = 169.0–175.2), at which an unstable limit cycle did not appear. However, because drastic vertical divergent vibrations appeared at U = 12 m/s for W/D = 3.0–5.0 and S/D = 0.0, the responses at these arrangements at U = 8 or 10 m/s are shown instead. Consequently, vertical predominant vibrations were observed at W/D = 2.5–9.5 in tandem arrangements (S/D = 0.0), which is a well-known WG phenomenon. Although Toriumi et al. (1999) and Miyata et al. (2000) indicated that WG occurs at $W/D \leq 6.0$, a 1DOF vertical predominant vibration was observed even at W/D = 9.5 in this study. Furthermore, vertical predominant vibrations were observed at W/D = 2.5–4.5, with a comparatively small S/D corresponding to the arrangements, in which Miyata et al. (2000) reported that WG appeared despite $S/D \neq 0.0$. Furthermore, 2DOF vertical and horizontal coupled vibrations, which should be WIFs, were observed at staggered arrangements at a comparatively large distance where WIFs might appear (Cooper and Wardlaw, 1971; Miyata et al., 2000). Unsteady 2DOF vibrations, including momentary zero amplitudes, were observed in all the 2DOF vibrations. This condition might be caused by the Kármán vortex shedding from the upstream cylinder, which fluctuated the coupled aerodynamic forces acting on the downstream cylinder. For the staggered arrangement with a large *S*/*D*, the trajectories of the 2DOF vibrations were in-phase elliptical orbits. Meanwhile, for a staggered arrangement with a small *S*/*D*, the trajectories were anti-phase elliptical orbits.

Notably, for the arrangement of (*X/D* = 3.0; *Y*/*D* = 0.5), the downstream cylinder showed two different responses depending on the wind velocity. To further understand the WIV characteristics, the contributing factors are discussed in Section 4.

To summarize, in terms of the arrangement of the two cylinders, the response of the downstream cylinder is classified as a vertical 1DOF, 2DOF in-phase, or 2DOF anti-phase vibration, as shown in Fig. 4. Some arrangements where vertical 1DOF or 2DOF vibrations occurred were not included in the arrangements in which WG or WIF occurred (Cooper and Wardlaw, 1971; Toriumi et al., 1999; Miyata et al., 2000).

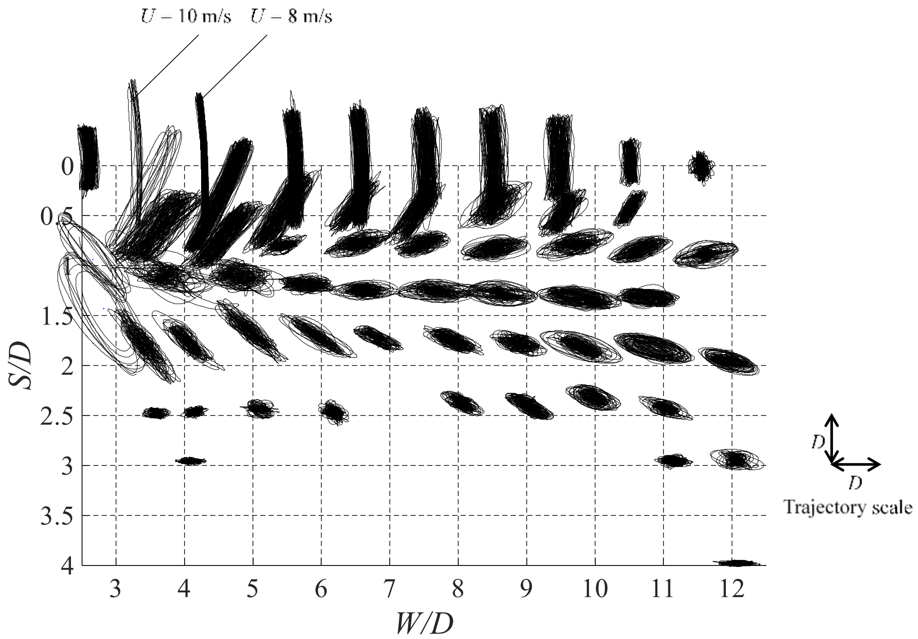

Fig. 3 Trajectories of the downstream cylinder at U = 12 m/s

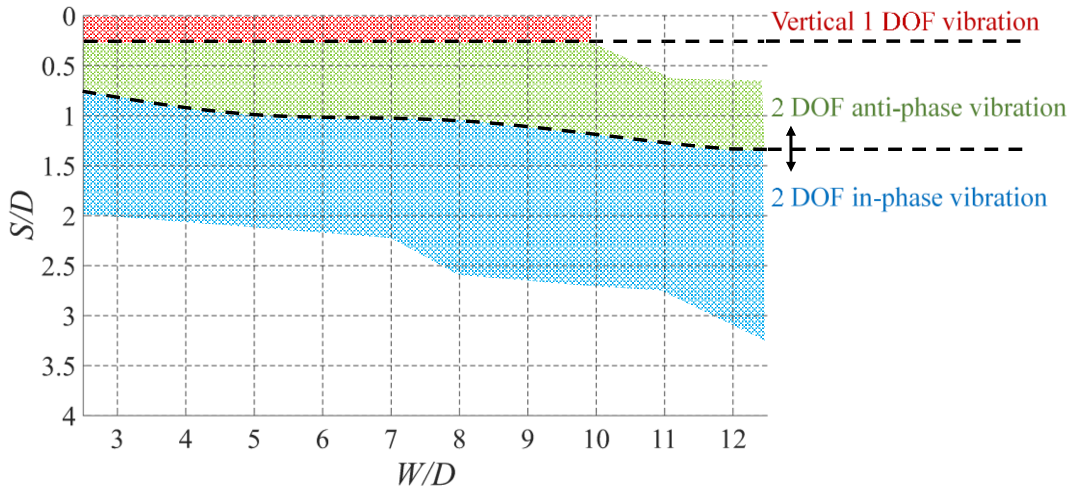

Fig. 4 Classification of the trajectories of the downstream cylinder in the spring-supported free vibration tests at U = 12 m/s

3.2 Unsteady aerodynamic forces acting on the downstream cylinder

To calculate the flutter derivatives, 1DOF forced vibration tests were conducted, as described in Section 2.2. Figs. 5–7 show examples of flutter derivatives with an evaluation time of 3 min. Fig. 7 shows H_1* at each vibration amplitude, where H_1* indicates a significant dependence on the vibration amplitude among the eight flutter derivatives. This amplitude dependency was observed in the results of H_1* and P_1*, which were obtained from the vertical forced vibration tests. No significant amplitude dependency was observed for the other six derivatives. This is likely because the downstream cylinder under the vertical vibration crossed the wake streamline from the upstream cylinder, unlike in the case of a horizontal vibration. Hence, the vertical wind velocity component may have induced an amplitude dependency.

The appearance of vertical vibrations can be evaluated based on H_1*, which reflects the vertical aerodynamic damping. Here, H_1* > 0 indicates a negative vertical aerodynamic damping. Hence, it can be assumed that vertical vibrations occur when H_1* > 0. Table 2 shows the vibration responses and H_1* of the representative cases based on Fig. 4. Case 1 represents WG in a tandem arrangement, which can be explained by H_1* > 0. Case 2 describes a vertically predominant vibration in the staggered arrangements with a combination of relatively small W/D and S/D values. This case is also characterized by H_1* > 0, as in Case 1, although some horizontal vibrations were included. Hence, despite the difference between the 1DOF and 2DOF cases, the vertical predominant vibrations in Cases 1 and 2 are excited by the negative vertical aerodynamic damping. Based on the generation mechanism, these vibrations are categorized as "vertical flutter," which corresponds to the WG by Miyata et al. (2000). However, the 2DOF vibrations in Cases 3–

6 cannot be explained by one flutter derivative because of coupled vibrations, as discussed in the following sections.

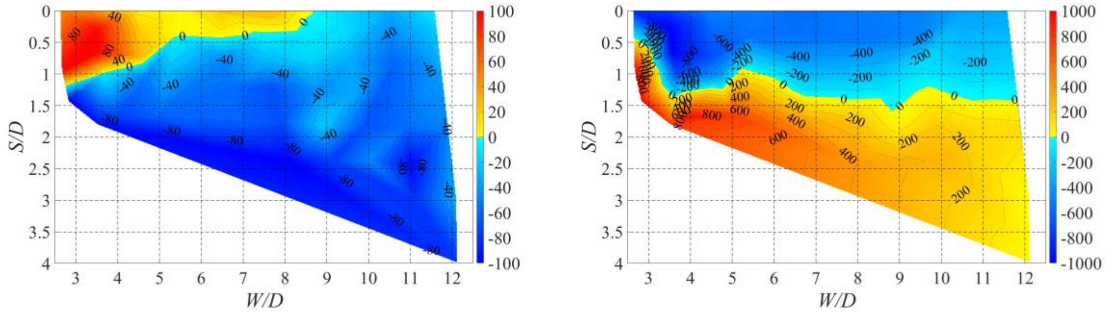

(a) (b)

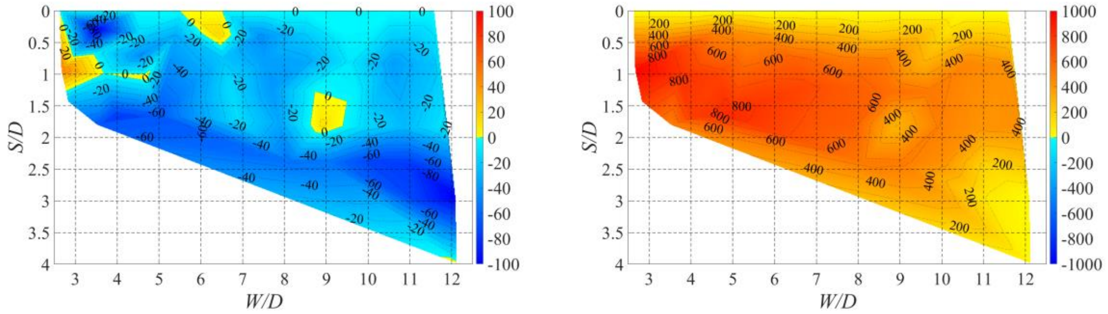

(c) (d)

Fig. 5 Flutter derivatives from the vertical 1DOF forced vibration test ($2A_\eta/D$ = 0.2) at U = 12 m/s (U/fD = 177.8): (a) H_1*, (b) H_4*, (c) P_1*, and (d) P_4*

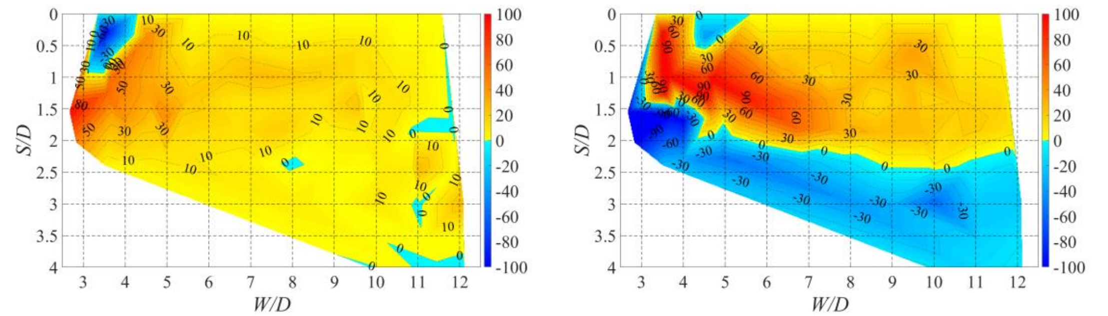

(a) (b)

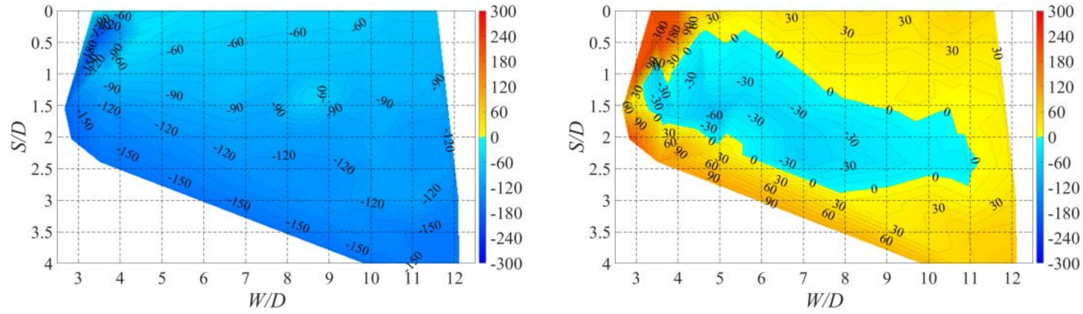

(c) (d)

Fig. 6 Flutter derivatives from the horizontal 1DOF forced vibration test ($2A_{\xi}/D = 0.8$) at $U = 12$ m/s ($U/fD = 177.8$): (a) H_5*, (b) H_6*, (c) P_5*, and (d) P_6*

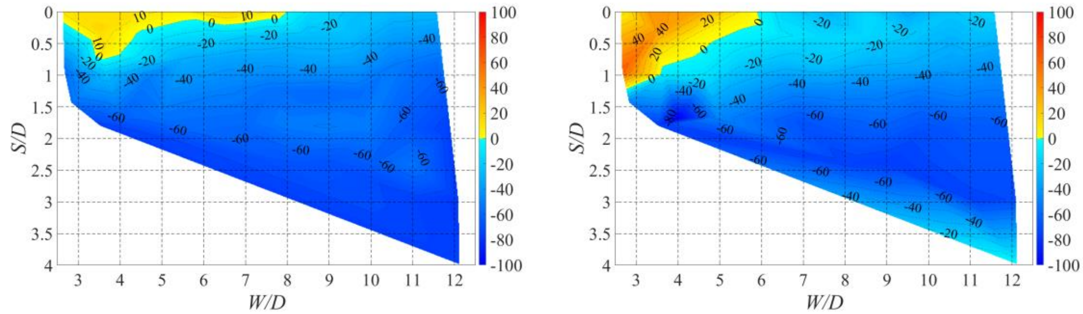

(a) (b)

Fig. 7 Flutter derivative H_1* at $U = 12$ m/s ($U/fD = 177.8$): (a) $2A_{\eta}/D = 1.2$ and (b) $2A_{\eta}/D = 2.4$

Table 2 Mechanisms of vibration at U = 12 m/s (U/fD = 177.8) evaluated from H_1*

Case	Arrangement of two cylinders		Amplitude for forced vib.		Free vib. Response		Derivative	Generation mechanism of vib.
	W/D	S/D	$2A_\xi/D$	$2A_\eta/D$	Amp. ratio η/ξ	Phase $\psi_{\xi\eta}$	H_1* (3 min.) $Lift$ - $\dot{\eta}$	
1	3.34	0.00	0.2	2.4	vertical divergent vib.		42.39	Vertical
2	3.50	0.30	1.6	2.4	1.53	anti-phase	41.14	Vertical
3	3.52	1.80	0.8	1.2	1.05	in-phase	−73.13	unknown
4	6.53	0.76	0.8	0.2	0.46	anti-phase	−44.27	unknown
5	9.71	1.29	0.8	0.2	0.27	in-phase	−33.59	unknown
6	11.11	2.98	0.8	0.2	0.33	in-phase	−78.54	unknown

3.3 Flutter analyses using unsteady aerodynamic forces

As clarified in the previous section, 1DOF and 2DOF vertically predominant vibrations were caused by a negative vertical aerodynamic damping (H_1* > 0) and can be defined as vertical flutter in terms of the generation mechanism. To clarify the generation mechanisms of the 2DOF coupled vibrations, 2DOF flutter analyses (complex eigenvalue analyses) were conducted in this study using flutter derivatives obtained from the forced vibration tests. The equations of motion of the downstream cylinder in the horizontal and vertical 2DOF conditions are written as Eqs. (5) and (6) using the aerodynamic forces described in Eqs. (2) and (3), respectively.

$$m\ddot{\xi} + c\dot{\xi} + k_\xi \xi = Drag \ , \qquad (5)$$

$$m\ddot{\eta} + c\dot{\eta} + k_\eta \eta = Lift \ , \qquad (6)$$

where c is the structural damping constant per unit length [kg/m·s] and k_ξ and k_η are the spring constants per unit length [N/m^2].

By applying flutter analyses to these equations, the logarithmic decrement (δ), frequency (f), amplitude ratio (η/ξ), and phase ($\psi_{\xi\eta}$) can be obtained. Here, $\delta < 0$ indicates that the system is aerodynamically unstable, and η/ξ and $\psi_{\xi\eta}$ represent the shapes of the vibration trajectory. The structural parameters were the same as those of the spring-supported free-vibration test results. Because the flutter derivatives depended on the oscillation amplitude, those obtained by the oscillation amplitude and closest to the spring-supported free vibration test results were selected for each arrangement.

Table 3 shows the flutter analysis results using the flutter derivatives of U = 12 m/s (U/fD = 177.8) for Cases 3–6, the vibration mechanisms of which are not explained in Section 3.2. The results of the flutter analyses showed that in-phase horizontal predominant vibrations appeared in the case of W/D = 2.5–5.0 and S/D = 1.2–2.0, including Case 3, which agreed well with the results of the spring-supported free vibration tests. Hereafter, the 2DOF coupled vibration at these arrangements where vibrations are explained by the 2DOF flutter analyses is known as "coupled flutter" based on its generation mechanism.

In addition, considering the phase ($\psi_{\xi\eta}$), the coupled flutter represented by Case 3 is denoted as "in-phase coupled flutter" herein.

Meanwhile, the arrangements where the 2DOF coupled vibration appeared in the spring-supported free vibration tests represented by Cases 4–6 showed no vibrations in the flutter analyses. The contributing factors are discussed in the next section.

Table 3 Results of the flutter analyses using flutter derivatives at U = 12 m/s (U/fD = 177.8)

Case	Arrangement of two cylinders		Amplitude for forced vib.		Free vib. Response		Results of flutter analyses				Generation mechanism of vib.
	W/D	S/D	$2A_\xi/D$	$2A_\eta/D$	Amp. ratio η/ξ	Phase $\psi_{\xi\eta}$	Log. Decrement δ [-]	Freq. f [Hz]	Amp. ratio η/ξ	Phase $\psi_{\xi\eta}$ [deg.]	
3	3.52	1.80	0.8	1.2	1.05	in-phase	−0.074	1.18	1.02	33.45 in-phase	In-phase coupled
4	6.53	0.76	0.8	0.2	0.46	anti-phase	0.070	1.34	0.10	−33.83 in-phase	Unknown
5	9.71	1.29	0.8	0.2	0.27	in-phase	0.032	1.31	0.23	−14.39 in-phase	Unknown
6	11.11	2.98	0.8	0.2	0.33	in-phase	0.116	1.30	1.28	−59.94 in-phase	Unknown

3.4 Contribution of flutter derivatives to the 2DOF vibration

Under a 2DOF coupled vibration, the aerodynamic coupling terms H_5*, H_6*, P_1*, and P_4* are critical. In the previous section, the flutter analyses did not elucidate all the 2DOF coupled vibrations that occurred in the spring-supported free vibration tests. This outcome is likely due to the unsteadiness of the 2DOF coupled vibrations, as shown in Fig. 3, caused by the time variations of the aerodynamic forces or flutter derivatives.

To evaluate the contribution of the flutter derivatives to the 2DOF coupled vibrations, additional flutter analyses focusing on one flutter derivative were conducted at U > 12 m/s (U/fD = 177.8) in staggered arrangements, where unstable responses were not observed in the previous flutter analyses represented by Cases 4–6. The flutter derivative was virtually obtained by increasing it linearly with respect to the reduced wind velocity, whereas the other flutter derivatives were obtained at U = 12 m/s. Table 4 shows the onset wind velocities U_{on} in this parametric study of flutter analyses for the arrangements of Cases 4–6. A low U_{on} indicates that the flutter derivative of interest contributes to the 2DOF vibrations. Clearly, the combination of a large positive P_4* and a large positive H_5* is crucial for inducing 2DOF vibrations. Occasionally, flutter can be induced by a combination of a large positive P_4* and negative H_6*. Although a large negative P_1* might induce 2DOF vibrations, the contribution of P_1* appeared to be much smaller than those of P_4*, H_5*, and H_6*. To summarize, 2DOF vibrations were induced by {P_4* > 0 and H_5* > 0} or {P_4* > 0 and H_6* < 0}.

Table 4 Onset wind velocities in the parametric studies of flutter analyses

Case	Arrangement of two cylinders		Amplitude for forced vib.		Flutter derivative of concern (at U = 12 m/s, U/fD = 177.8) **Onset wind velocity U_{on} [m/s]**							
	W/D	S/D	$2A_\xi/D$	$2A_\eta/D$	H_1* *Lift* - $\dot{\eta}$	H_4* *Lift* - η	P_1* *Drag* - $\dot{\eta}$	P_4* *Drag* - η	H_5* *Lift* - $\dot{\xi}$	H_6* *Lift* - ξ	P_5* *Drag* - $\dot{\xi}$	P_6* *Drag* - ξ
4	6.53	0.76	0.8	0.2	−44.27 **Stable**	−385.03 **Stable**	−21.28 **Stable**	627.22 **34.5**	22.78 **28.5**	33.41 **Stable**	−70.91 **Stable**	−13.02 **Stable**
5	9.71	1.29	0.8	0.2	−33.59 **Stable**	36.41 **Stable**	−4.50 **Stable**	530.93 **39.5**	8.06 **23.0**	17.55 **Stable**	−47.10 **Stable**	3.86 **Stable**
6	11.11	2.98	0.8	0.2	−78.54 **Stable**	155.27 **Stable**	−71.11 **152.5**	84.04 **98.0**	−0.62 **Stable**	−19.46 **74.5**	−114.41 **Stable**	13.45 **Stable**

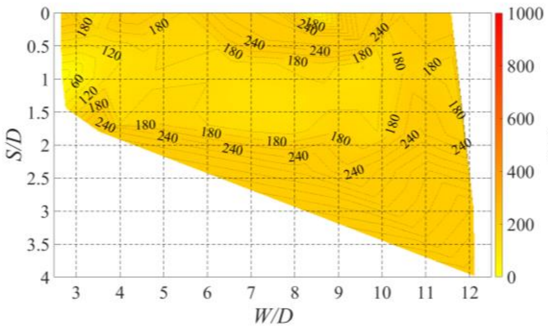

(a)

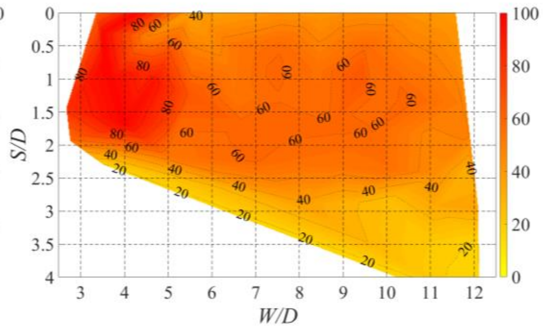

(b)

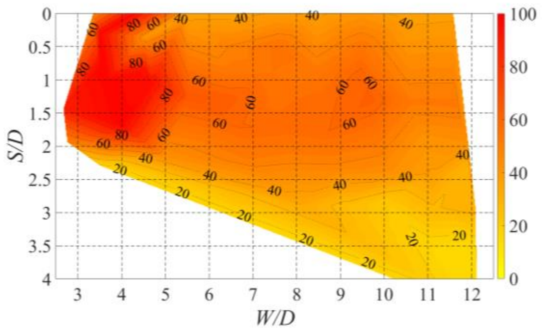

(c)

Fig. 8 Standard deviations of flutter derivatives at U = 12 m/s (U/fD = 177.8): (a) P_4* ($2A_\eta/D$ = 0.2), (b) H_5* ($2A_\xi/D$ = 0.8), and (c) H_6* ($2A_\xi/D$ = 0.8)

Fig. 8 shows the standard deviations of the flutter derivatives. As shown in Figs. 5, 6, and 8, P_4* is approximately positive at any arrangement, although the signs of H_5* and H_6* easily change with respect to the arrangement and time. The fact that flutter did not occur is attributable to the time variations of H_5* or H_6*. The flutter derivatives used for the flutter analyses in Section 3.3 were based on aerodynamic forces for 3 min, which corresponded to 243-cycle oscillations. Therefore, considering the unsteadiness of the flutter derivatives, particularly H_5* and H_6*, flutter analyses based on short-time-averaged flutter derivatives were conducted to determine whether they could elucidate the mechanisms of 2DOF vibrations. Hence, the periods at $H_5^* > 0$ and $H_6^* < 0$ are emphasized. Table 5 shows an example of the flutter analysis results with a short evaluation time.

First, the 10-cycle-averaged H_5^* was calculated, and a positive value was used for the flutter analyses. The results show that in-phase horizontal predominant vibrations appeared in the case of staggered arrangements represented by Cases 4-i and 5, although no vibrations appeared in Case 6-i. Regarding the arrangements represented by Case 5, the flutter analyses and spring-supported tests exhibited 2DOF in-phase vibrations, and the amplitude ratios showed a good agreement with each other. Therefore, the vibration at these arrangements, including that of Case 5, can be called “in-phase coupled flutter,” as in Case 3. However, the arrangements represented by Case 4 showed 2DOF anti-phase vibrations in the spring-supported free vibration tests, unlike the flutter analysis results.

Next, the 10-cycle-averaged H_6^* was calculated, and a negative value was used for the flutter analyses of the arrangements, as represented by Cases 4 and 6. The flutter analysis results for the arrangements, including those of Case 4-ii, showed 2DOF anti-phase vibrations, and they were the same as those of the spring-supported free vibration tests. Hence, they can be termed “anti-phase coupled flutter.”

By considering the short-time-averaged H_5^* and H_6^*, the vibrations obtained from the spring-supported free vibration tests at the arrangements represented by Cases 4 and 5 are described well. However, the vibration responses of Case 6 are not explained in this manner.

Fig. 9 shows all results mentioned above to obtain the relationship between the arrangements of parallel cylinders and the generation mechanisms of the WIVs. As shown, vertical flutter caused by $H_1^* > 0$ appeared in the tandem arrangements or a comparatively small spacing ratio, whereas coupled flutter appeared in a comparatively large spacing ratio. The area of the coupled flutter can be segmented into anti-phase coupled flutter in small S/D regions and in-phase coupled flutter in large S/D regions in terms of the contributions of P_4^*, H_5^*, and H_6^*. The generation mechanisms cannot explain the vibrations in the case of (W/D = 6.0–9.5; $S/D \approx 0.3$). These arrangements refer to the boundary between the vertical flutter and anti-phase coupled flutter. With these arrangements, the results of the spring-supported free vibration tests showed unsteady responses. This outcome is probably attributed to H_1^* having positive or negative values over time owing to a significant unsteadiness even if the time-averaged value of H_1^* is zero. Based on this figure, a classification map of the arrangements of two cylinders based on the WIV mechanisms is introduced, as shown in Fig. 10. The mechanisms of WIVs can be categorized into three types: vertical flutter, 2DOF in-phase flutter, and 2DOF anti-phase flutter.

Table 5 Results of the flutter analyses at $U = 12$ m/s ($U/fD = 177.8$) using flutter derivatives with a short evaluation period

Case	Arrangement of two cylinders		Amplitude for forced vib.		Free vib. response		Results of flutter analyses using flutter derivatives with a short evaluation period						Generation mechanism of vib.
	W/D	S/D	$2A_\xi/D$	$2A_\eta/D$	Amp. ratio η/ξ	Phase $\psi_{\xi\eta}$	Focused derivatives (Evaluation period)	Derivative with short evaluation period	Log. decrement δ [-]	Freq. f [Hz]	Amp. ratio η/ξ	Phase $\psi_{\xi\eta}$ [deg.]	
4—i	6.53	0.76	0.8	0.2	0.46	anti-phase	$H_5^* > 0$ (10 cycles)	H_5^* (49.93) H_6^* (9.13)	−0.004	1.34	0.12	−72.32 in-phase	Unknown
4—ii							$H_6^* < 0$ (10 cycles)	H_5^* (37.22) H_6^* (−17.23)	−0.027	1.36	0.11	254.67 anti-phase	Anti-phase coupled
5	9.71	1.29	0.8	0.2	0.27	in-phase	$H_5^* > 0$ (10 cycles)	H_5^* (18.06) H_6^* (−15.64)	−0.105	1.33	0.24	−61.66 in-phase	In-phase coupled
6—i	11.11	2.98	0.8	0.2	0.33	in-phase	$H_5^* > 0$ (10 cycles)	H_5^* (12.00) H_6^* (-17.57)	0.111	1.29	1.24	−81.07 in-phase	Unknown
6—Ii							$H_6^* < 0$ (10 cycles)	H_5^* (1.62) H_6^* (−30.49)	0.097	1.30	1.30	-84.61 in-phase	Unknown

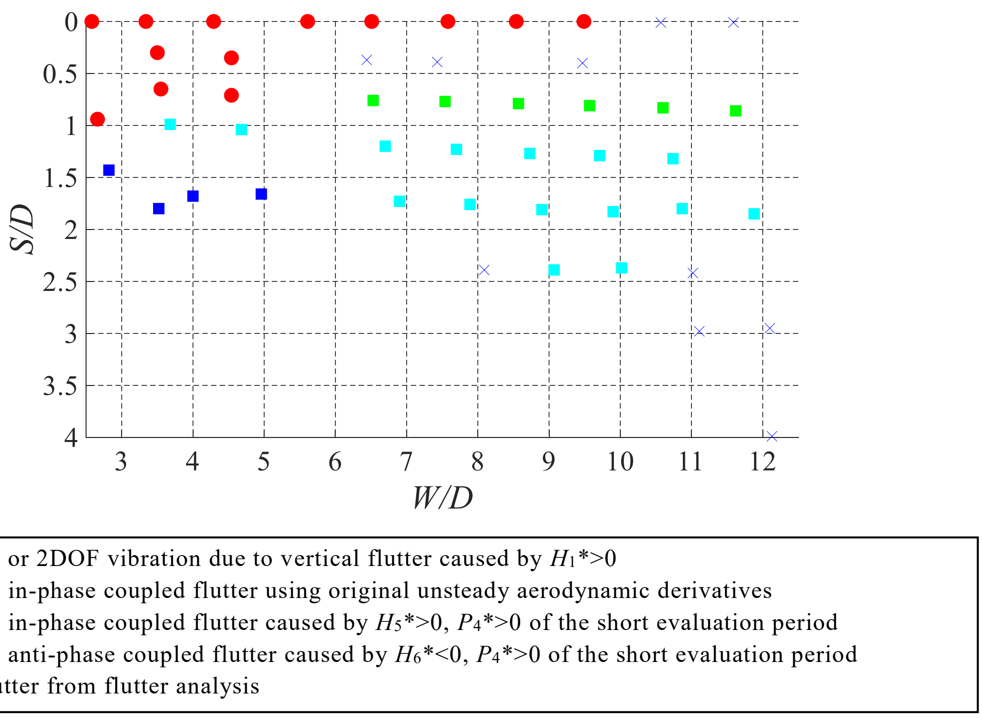

Fig. 9 Results of the flutter analyses at $U = 12$ m/s ($U/fD = 177.8$)

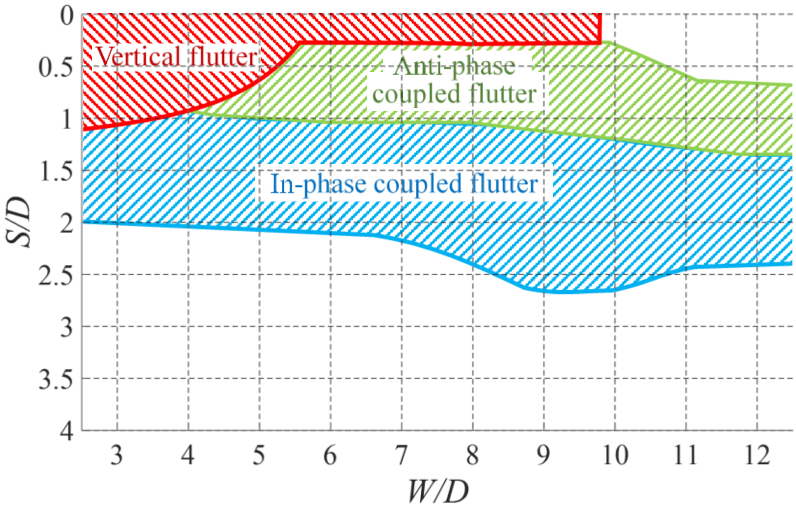

Fig. 10 Classification of vibration mechanisms based on flutter analyses at U = 12 m/s (U/fD = 177.8): Vertical flutter, vertical flutter caused by $H_1^* > 0$; anti-phase coupled flutter, 2DOF anti-phase coupled flutter caused by $H_6^*<0$, $P_4^*>0$ of the short evaluation period; in-phase coupled flutter, 2DOF in-phase coupled flutter caused by the original unsteady aerodynamic derivatives or $H_5^*>0$, $P_4^*>0$ of the short evaluation period

3.5 Quasi-steady theory application

Several researchers (Simpson, 1971; Simpson and Flower, 1977; Price and Adballah, 1990; Deng et al., 2019) have recently attempted to clarify the mechanisms of WIVs using a quasi-steady approach and concluded that the quasi-steady approach can reflect the characteristics of WIVs in certain arrangements of two cylinders. However, the quasi-steady theory cannot clearly describe WIVs well when two cylinders are closely arranged (Shiraishi et al., 1984; Knisely and Kawagoe, 1990). In this study, time-history response analyses using the quasi-steady theory were conducted to determine the applicability of the quasi-steady theory. Using the quasi-steady theory, the aerodynamic forces acting on the downstream cylinder can be expressed as Eqs. (7)–(14), based on the concepts of Simpson (1971), as shown in Fig. 11.

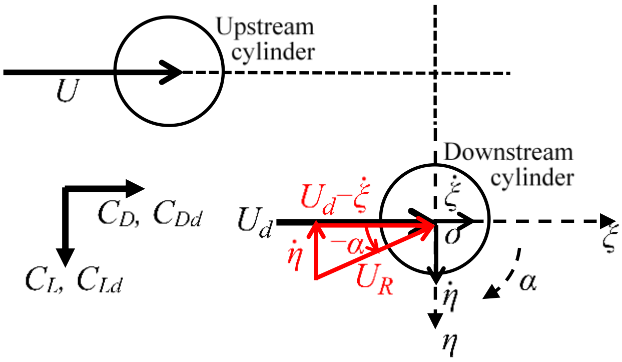

Fig. 11 Velocities and forces from the quasi-steady model

The aerodynamic forces acting on the downstream cylinder (*Drag* and *Lift*) can be written as

$$Drag = \frac{1}{2}\rho U_R{}^2 D\ \ (C_{Dd}\cos\alpha - C_{Ld}\sin\alpha)\text{ , and} \tag{7}$$

$$Lift = \frac{1}{2}\rho U_R{}^2 D\ \ (C_{Dd}\sin\alpha + C_{Ld}\cos\alpha)\quad , \tag{8}$$

where U_d is the local wind velocity at the downstream cylinder, U_R is the relative wind velocity at the downstream cylinder, and C_{Dd} and C_{Ld} are the drag and lift coefficients defined by U_d, respectively. By introducing the relative wind velocity ratio h (= U_d/U), C_{Dd} and C_{Ld} can be written as follows:

$$C_{Dd} = C_D\frac{U^2}{U_d{}^2} = \frac{C_D}{h^2}\text{ , and} \tag{9}$$

$$C_{Ld} = C_L\frac{U^2}{U_d{}^2} = \frac{C_L}{h^2}\ . \tag{10}$$

In addition, by considering $\alpha << 1$ and disregarding the higher-order terms, Eqs. (7) and (8) can be written as follows:

$$Drag = \frac{1}{2}\rho U^2 D\left(\frac{C_L}{hU}\dot{\eta} - \frac{2C_D}{hU}\dot{\xi} + C_D\right)\text{ , and} \tag{11}$$

$$Lift = \frac{1}{2}\rho U^2 D\left(-\frac{C_D}{hU}\dot{\eta} - \frac{2C_L}{hU}\dot{\xi} + C_L\right). \tag{12}$$

For a small motion, Eqs. (9) and (10) can be linearized as follows:

$$m\ddot{\xi} + c\dot{\xi} + k_\xi \xi = \frac{1}{2}\rho U^2 D\left(\frac{C_L}{hU}\dot{\eta} + \frac{\partial C_D}{\partial \eta}\eta - \frac{2C_D}{hU}\dot{\xi} + \frac{\partial C_D}{\partial \xi}\xi\right), \text{ and} \tag{13}$$

$$m\ddot{\eta} + c\dot{\eta} + k_\eta \eta = \frac{1}{2}\rho U^2 D\left(-\frac{C_D}{hU}\dot{\eta} + \frac{\partial C_L}{\partial \eta}\eta - \frac{2C_L}{hU}\dot{\xi} + \frac{\partial C_L}{\partial \xi}\xi\right). \tag{14}$$

In this study, the relative wind velocity ratio h can be calculated based on C_{Dd} and C_D using Eq. (9). The value of C_{Dd} was assumed to be 1.2, based on the drag coefficient of a single cylinder under the subcritical *Re* region (Simpson, 1971), and C_D was directly measured in this study, as described below.

The drag and lift forces at each arrangement were measured to calculate C_D and C_L by conducting vertical 1DOF forced vibration tests with a low vibration frequency of f = 0.027 Hz. Fig. 12 shows the results of C_D and C_L for each arrangement of the two cylinders ($Re = 4.1 \times 10^4$), which were similar to those measured by Zdravkovich and Pridden (1977) ($Re = 6.0 \times 10^4$) and Assi et al. (2013) ($Re = 1.9 \times 10^4$) obtained under static conditions. Although *Re* used by Zdravkovich and Pridden (1977), Assi et al. (2013), and the present study are different from one another, the static coefficients are almost the same. Thus, the effect of *Re* is probably negligible under the subcritical *Re* range ($Re = 10^4$–10^6). Therefore, calculating C_D and C_L by conducting vertical 1DOF forced vibration tests with a low vibration frequency is considered appropriate. Moreover, C_D and C_L, which were uninterrupted in the arrangements of the two cylinders, were obtained.

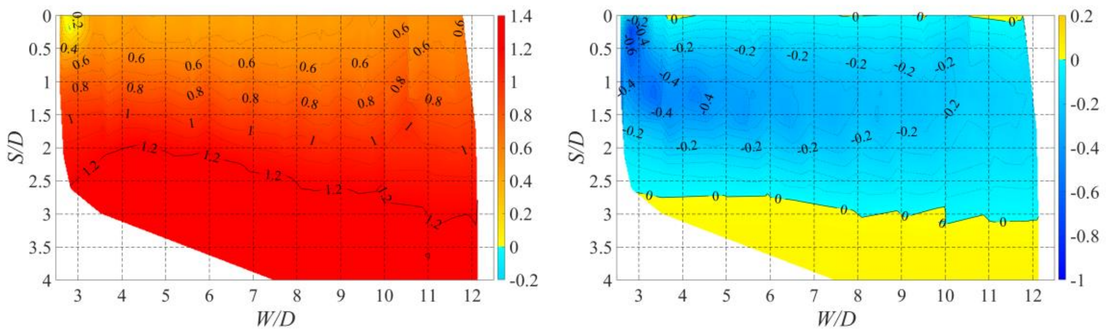

(a) (b)

Fig. 12 Contour diagrams of aerostatic force coefficients at U = 12 m/s (U/fD = 177.8): (a) C_D and (b) C_L

Using the obtained C_D and C_L, time-history response analyses were conducted using the classical Runge–Kutta method to solve Eqs. (13) and (14) for the arrangements in which the in-phase and anti-phase coupled flutter appeared in the flutter analyses. Fig. 13 shows the constant orbits of the downstream cylinder calculated from the time-history response analyses. When the two cylinders were arranged in a far staggered arrangement (W/D = 6.0–12.0; S/D =1.0–2.0), the trajectories from the quasi-steady theory showed anti-clockwise elliptical shapes. These trajectories agreed well with the results of spring-supported free vibration tests and flutter analyses. In addition, the values of η/ξ and $\psi_{\xi\eta}$ obtained from the time-history response analyses using the quasi-steady theory, flutter analyses, and spring-supported free vibration tests were similar. Hence, the vibrations at these arrangements were explained well through the quasi-steady theory. Although steady-state responses were also calculated for the comparatively close arrangements, the calculated amplitude and η/ξ significantly differed from the spring-supported free vibration tests. Vibrations at arrangements where the quasi-steady theory was applicable likely exhibited weak unsteadiness. However, almost all the time-history analysis results for quasi-steady applicable arrangements exhibited smaller amplitudes than the spring-supported free vibration responses, as indicated by Deng et al. (2019). Although the accuracy of calculating the amplitude using the quasi-steady theory can be further improved, the range within which the vibrations were explained based on the quasi-steady theory was clarified.

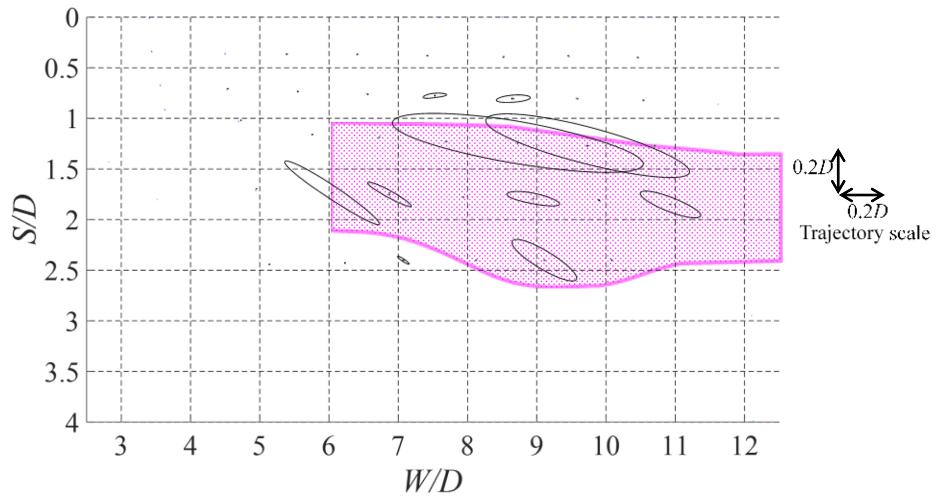

Fig. 13 Trajectories of the downstream cylinder calculated from the time-history analyses at U = 12 m/s (U/fD = 177.8)

3.6 Classification map of the generation mechanisms of WIVs

Fig. 14 shows the classification map of the WIV based on all discussions, including the vibration responses shown in Fig. 4, the generation mechanisms of WIVs based on the unsteady aerodynamic forces shown in Fig. 10, and the quasi-steady applicable arrangements shown in Fig. 13. The generation mechanisms for each arrangement and their boundaries are clearly explained. Fig. 14 shows the correspondence between the generation mechanisms and WIV responses in various arrangements of the two cylinders. The generation mechanisms were categorized into vertical flutter, which was caused by $H_1^* > 0$, and coupled flutter, which exhibited different phase characteristics as determined by the contribution of either H_5^* or H_6^* and the different applicability of the quasi-steady theory. In terms of the classification map based on the generation mechanisms, WG and WIF must be explained as vertical and coupled flutter, respectively. However, the 2DOF vibration in the staggered arrangements with a comparatively close spacing ratio is vertical flutter in terms of the generation mechanisms.

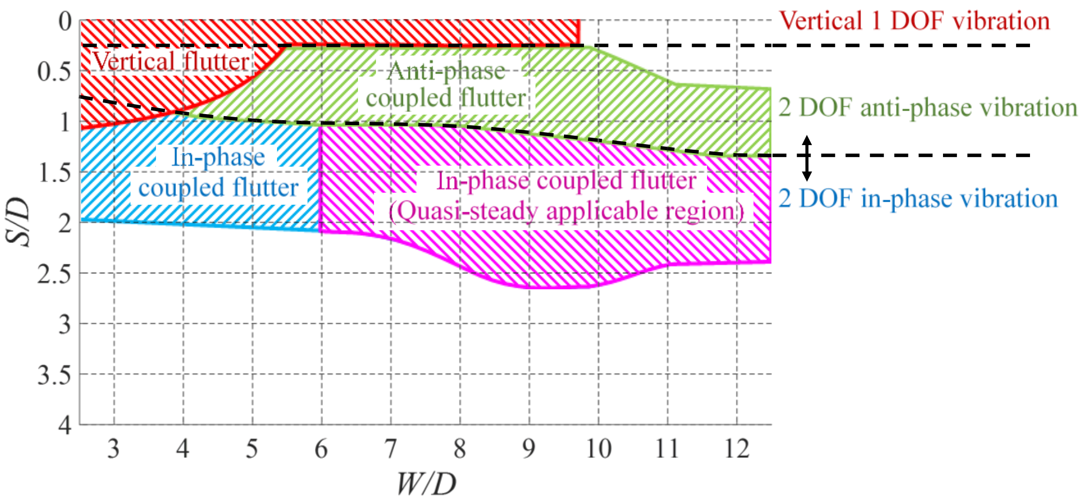

Fig. 14 Classification map of WIVs at $U = 12$ m/s ($U/fD = 177.8$): Vertical flutter, vertical flutter caused by $H_1^* > 0$; anti-phase coupled flutter, 2DOF anti-phase coupled flutter caused by $H_6^* < 0$, $P_4^* > 0$ of a short evaluation period; in-phase coupled flutter, 2DOF in-phase coupled flutter caused by the original unsteady aerodynamic derivatives or $H_5^* > 0$, $P_4^* > 0$ of a short evaluation period

4. Wind velocity dependency of WIVs

As reported in Section 3, a classification map of WIVs was developed based on a series of wind tunnel tests and analyses under the subcritical Re range ($Re = 4.1 \times 10^4$; $U =$

12 m/s). Meanwhile, different types of vibrations for different wind velocities were discovered at (X/D = 3.0; Y/D = 0.5) even under the subcritical Re range. Fig. 15 shows the velocity–amplitude diagrams at (X/D = 3.0; Y/D = 0.5), which exhibited 2DOF vibrations at U = 1–3 m/s ($Re = 3.4 \times 10^3$–1.0×10^4; U/fD = 15.2–45.5) and predominantly vertical vibrations at U = 6–12 m/s ($Re = 2.1 \times 10^3$–4.1×10^4; U/fD = 90.9–182). To investigate the causes of this wind velocity dependency on WIVs, forced vibration tests and flutter analyses were conducted with arrangements around (W/D = 3.0; S/D = 0.5). Considering the equilibrium position change of the downstream cylinder and the change in flutter derivatives with reduced wind velocity, the wind velocity dependency of WIVs is discussed. The effect of Re was negligible because all tests were conducted in the subcritical Re range.

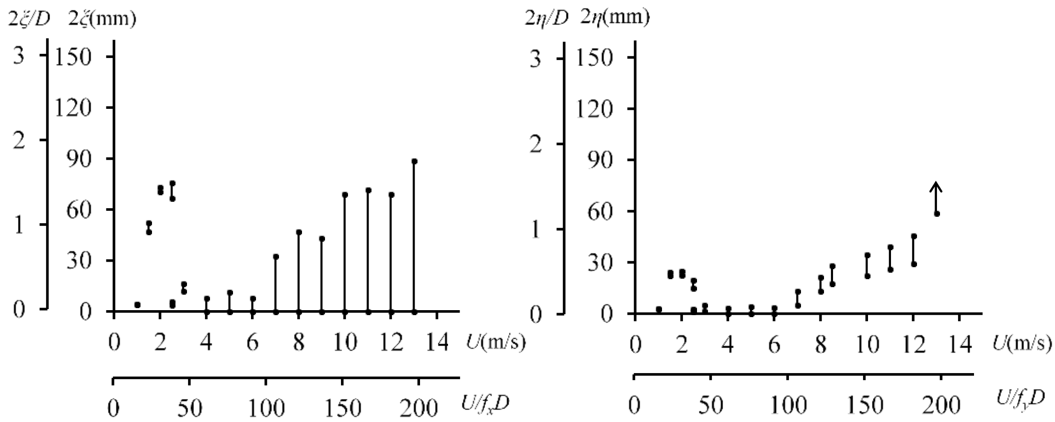

Fig. 15 Velocity–amplitude diagrams at (X/D = 3.0; Y/D = 0.5) from the spring-supported free vibration test

4.1 Effects of static displacement

In this section, the arrangement of (X/D = 3.0; Y/D = 0.5) is emphasized considering the apparent wind velocity dependency of the vibrations. Fig. 16 shows the equilibrium position (static displacement) of the downstream cylinder for each approaching wind velocity (U = 0–12 m/s) obtained from the spring-supported free vibration tests. A static displacement in the vertical direction was observed for $U < 6$ m/s, and a static displacement in the horizontal direction was observed for $U \geq 6$ m/s. Finally, static displacements of < 0.2D in each direction were discovered at U = 12 m/s. These static displacements may change the vibration mechanisms depending on the wind velocity.

To clarify the effects of the static displacement, 1DOF forced vibration tests focusing on a narrow range (W/D = 3.0–3.5; S/D = 0.0–0.5) were conducted under various wind velocity conditions. The forced vibration frequency was set to f = 1.32 Hz, and the double amplitude of the vibration was set to $2A$ = 20 mm ($2A/D$ = 0.4) in the horizontal and vertical directions, corresponding to the responses of the downstream cylinder in the spring-supported free vibration tests at (X/D = 3.0; Y/D = 0.5). Fig. 17 shows the vertical aerodynamic damping (H_1*), which is a key parameter for vertical flutter, at U = 3, 6, and 12 m/s (U/fD = 40.5, 90.9, and 182, respectively). In addition, the equilibrium positions were plotted. The value of H_1* considerably changed by a slight difference in the arrangement of the two cylinders, including the change in sign. The same tendency was observed for the other flutter derivatives. Furthermore, H_1* in some arrangements changed from negative to positive when the wind velocity increased. Considering the static displacement and H_1* characteristics as a function of wind velocity and arrangement, vibrations with different mechanisms were observed at different wind velocities. This result implies that even in the absence of static displacements, the vibration responses can change in some arrangements owing to the increase in the reduced wind velocity. Based on the generation mechanisms, the relationship between the vibration response and reduced wind velocity is further discussed in Section 4.2.

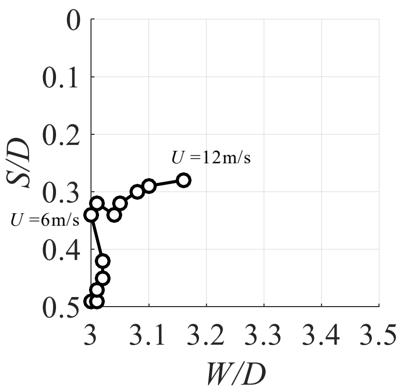

Fig. 16 Equilibrium position (static displacement) of the downstream cylinder at (X/D = 3.0; Y/D = 0.5)

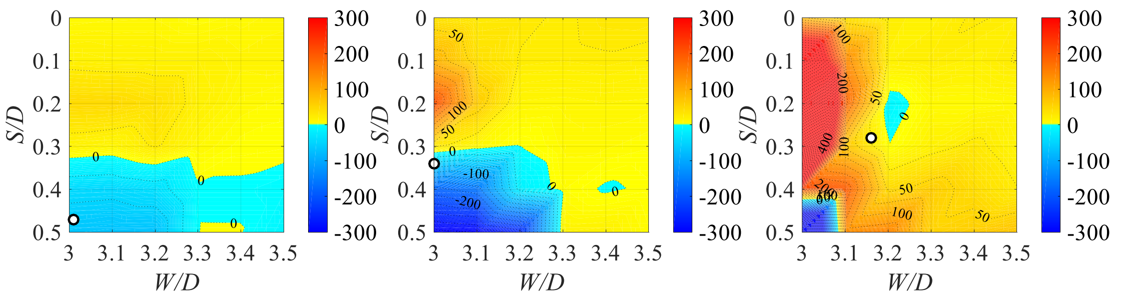

(a) (b) (c)

Fig. 17 Contour diagrams of H_1* ($2A_\eta/D$ = 0.4) (o, equilibrium position of the downstream cylinder): (a) U = 3 m/s (U/fD = 40.5), (b) U = 6 m/s (U/fD = 90.9), and (c) U = 12 m/s

(U/fD = 182)

4.2 Effects of reduced wind velocity

In this section, the investigation on the relationship between the reduced wind velocity and vibration mechanism through flutter analyses is discussed. In particular, the arrangement of (W/D = 3.0; S/D = 0.3) is emphasized, which was observed for $U \approx 6$ m/s (U/fD = 90.9), because H_1* significantly changed with the wind velocity, as shown in Fig. 17. The structural parameters were the same as those of the spring-supported free vibration tests, except for structural damping. The structural damping was set to zero to focus on the aerodynamic characteristics of the system. Fig. 18 shows the flutter analysis results for (W/D = 3.0; S/D = 0.3). The results of δ, η/ξ, and $\psi_{\xi\eta}$ indicate that in-phase horizontal predominant vibrations appeared at U = 1.0–2.5 m/s, whereas anti-phase vertical vibrations appeared at U = 2.5–4.3 m/s and U > 7.9 m/s. Therefore, the aerodynamic characteristics at (W/D = 3.0; S/D = 0.3) changed based on the wind velocity. Hence, the generation mechanisms of the WIVs differed at each reduced wind velocity.

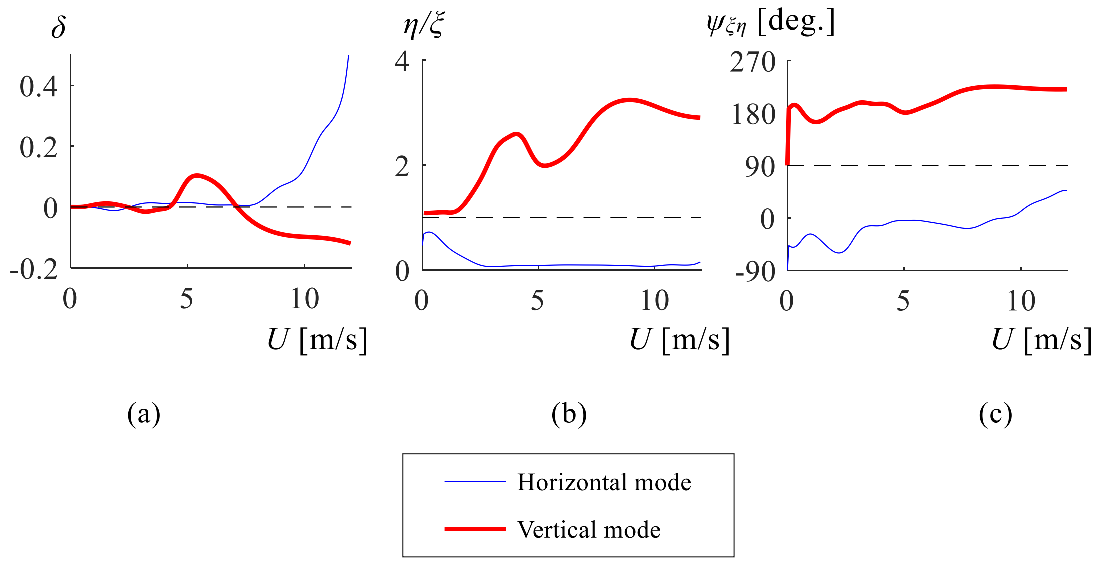

Fig. 18 Results of the flutter analysis at (W/D = 3.0; S/D = 0.3). (a) δ, (b) η/ξ, and (c) $\psi_{\xi\eta}$ [deg.]

To further investigate the generation mechanisms at each wind velocity based on the contribution of the flutter derivatives, additional flutter analyses were conducted by setting one flutter derivative to zero or three times its original value.

Fig. 19 shows the significant effects of H_1*, H_5*, and P_4* on δ. Regarding the horizontal vibration at U = 1.0–2.5 m/s, H_5* and P_4* significantly affected δ, whereas H_1* exerted the less effect. H_5* and P_4* induced a horizontal vibration at U = 1.0–2.5 m/s. Consequently, regarding the classification map, this vibration is regarded as in-phase coupled flutter, based on the discussion in Section 3. Meanwhile, vibrations at U = 2.5–4.3 m/s and U > 7.9 m/s were clearly induced by H_1*. Fig. 20 shows the value of H_1* obtained by the forced vibration tests. Here, H_1* indicated positive values at U/fD = 30–60 and U/fD > 90 (corresponding to U = 2.5–4.3 m/s and U > 7.9 m/s, respectively), signifying that these are vertical flutter.

In summary, considering the generation mechanisms of WIVs as mentioned in Section 3, it was clarified that the equilibrium position was slightly changed owing to the static displacement, and thus, different generation mechanisms were observed depending on the wind velocity. In-phase coupled flutter appeared at a low reduced wind velocity, whereas vertical flutter appeared at a high reduced wind velocity.

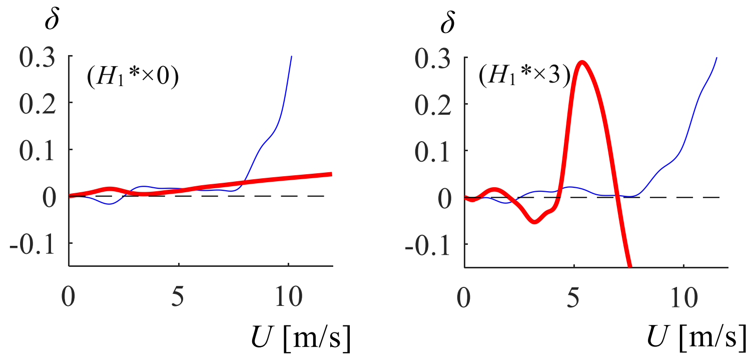

(a) (b)

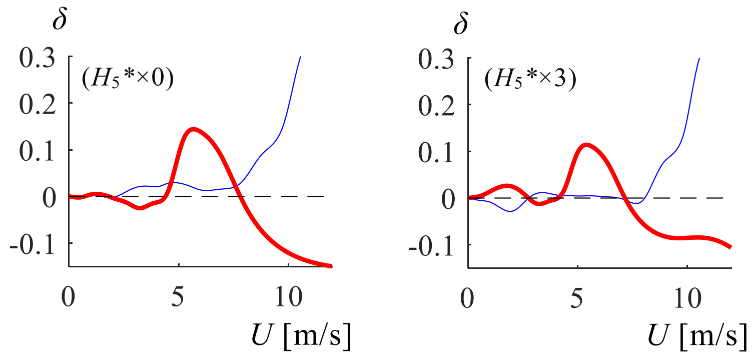

(c) (d)

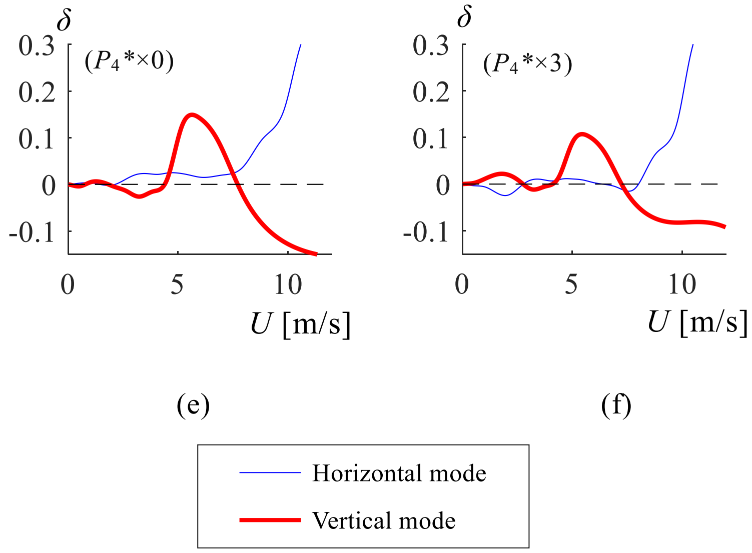

Fig. 19 Logarithmic decrement δ at (W/D = 3.0; S/D = 0.3) calculated through a flutter analysis using a virtually set parameter. (a) H_1^* × 0, (b) H_1^* × 3, (c) H_5^* × 0, (d) H_5^* × 3, (e) P_4^* × 0, and (f) P_4^* × 3

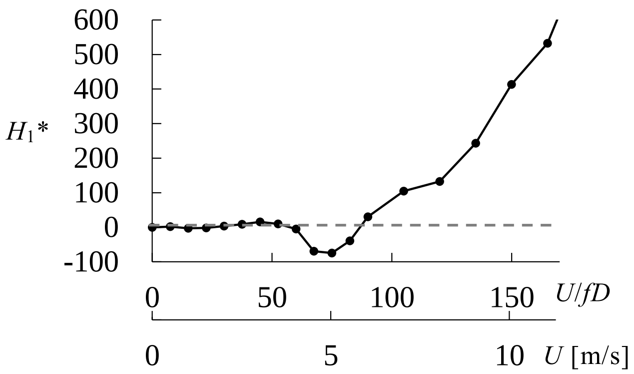

Fig. 20 H_1^* obtained from the forced vibration tests at (W/D = 3.0; S/D = 0.3; $2A_\eta/D$ = 0.4)

5. Conclusions

In this study, to classify the characteristics of WIVs in various arrangements of two circular cylinders, the generation mechanisms of WIVs in the subcritical region were investigated through wind tunnel tests, flutter analyses, and time-history analyses. The following conclusions were drawn:

1) The arrangement of two cylinders can be classified as a classification map in the area of vertical flutter caused by the negative vertical aerodynamic damping indicated by H_1^* > 0 and that of 2DOF coupled flutter caused by aerodynamic coupling indicated by P_4^*, H_5^*, and H_6^*. Furthermore, the coupled-flutter area can be segmented into

anti-phase coupled flutter, in-phase coupled flutter (quasi-steady applicable), and in-phase coupled flutter (quasi-steady inapplicable) areas depending on the contribution of either H_5* or H_6*.

2) Vertical predominant vibration (WG) corresponding to vertical flutter was observed at a horizontal distance of W/D = 2.5–9.5 (where D is the cylinder diameter) in tandem arrangements (vertical distance of S/D = 0.0). Moreover, a 2DOF coupled vibration with a small spacing ratio (W/D < 4.0 and S/D < 1.5) was classified as vertical flutter.
3) A 2DOF coupled vibration with a large spacing ratio (W/D > 6.0; S/D > 1.0) was considered in-phase coupled flutter, which can be explained by the quasi-steady theory.
4) When the two cylinders were closely arranged (W/D = 3.0; S/D = 0.3), in-phase coupled vibration and vertical predominant vibration occurred depending on the reduced wind velocity. Furthermore, the generation mechanisms of the WIVs around this arrangement were sensitive to slight differences in the distances between the two cylinders. The vibration responses may also drastically change owing to the static displacement of the downstream cylinder.

Acknowledgement

This study was partially supported by JSPS KAKENHI, Grant Number JP20H02232. The authors thank former students at Kyoto University for their contributions to this study.

Reference

Alam, M.M. and Kim, S. (2009). Free vibration of two identical circular cylinders in staggered arrangement. Japan Society of Fluid Mechanics and IOP Publishing Ltd Fluid Dynamics Research, 41(3).

Alam, M.M. and Meyer, J.P. (2013). Global aerodynamic instability of twin cylinders in cross flow, *J. Fluids Struct.*, 41, 135-145. https://doi.org/10.1016/j.jfluidstructs.2013.03.007

Assi, G. R. S., Bearman, P. W., Carmo, B. S., Meneghini, J. R., Sherwin, S. J., and Willden, R. H. J. (2013). The role of wake stiffness on the wake-induced vibration of the downstream cylinder of a tandem pair, *J. Fluid Mech*., 718, 210–245. https://doi:10.1017/jfm.2012.606

Assi, G.R.S., Bearman, P.W., and Meneghini, J.R. (2010). On the wake-induced vibration of tandem circular cylinder, *J. Fluid Mech.*, 661(4), 365-401. https://doi.org/10.1017/s0022112010003095

Brika, D. and Laneville, A. (1999). The flow interaction between a stationary cylinder and a downstream flexible cylinder, *J. Fluids Struct.*, 13(5), 579-606. https://doi.org/10.1006/jfls.1999.0220

Carmo, B.S., Sherwin, S.J., Bearman, P.W., and Willden, R.H.J. (2011). Flow-induced vibration of a circular cylinder subjected to wake interference at low Reynolds number, *J. Fluids Struct.*, 27,503–522. https://doi:10.1016/j.jfluidstructs.2011.04.003

Cooper, K. R. and Wardlaw, R. L. (1971). Aeroelastic Instabilities in Wakes. *Proceeding of the International Conference on Wind Effects on Buildings and Structures*, Tokyo, Japan, 647-655.

Deng, Y., Li, S., and Chen, Z. (2019). Unsteady theoretical analysis on the WIV of suspension bridge hangers, *J. Bridge Eng.*, 24(2). https://doi.org/10.1061/(asce)be.1943-5592.0001339

Fujino Y., Kimura, K., and Tanaka, H. (2012). Wind Resistance Design Codes of Bridges in Japan, *Wind Resistant Design of Bridges in Japan*, 1-7. https://doi.org/10.1007/978-4-431-54046-5_1

Hua, X.G., Chen, Z.Q., Lei, X., Wen, Q., and Niu, H.W. (2019). Monitoring and control of wind-induced vibrations of hanger ropes of a suspension bridge, *Smart Structures and Systems*, 23(6), 683–693.

Igarashi, T. (1981). Characteristics of the flow around two circular cylinders arranged in tandem: 1st Report, *Bulletin of JSME*, 24(188), 323-331. https://doi.org/10.1299/jsme1958.24.323

Kim, S., Alam, M.M., Sakamoto, H., and Zhou, Y. (2009). Flow-induced vibrations of two circular cylinders in tandem arrangement. Part 1: Characteristics of vibration., *J. Wind Eng. Ind. Aerodyn.*, 97, 304–311. https://doi.org/10.1016/j.jweia.2009.07.004

Knisely, C.W. and Kawagoe, M. (1990). Forced-displacement measurements on closely spaced tandem cylinders, *J. Wind Eng. Ind. Aerodyn.*, 33, 81-90. https://doi.org/10.1016/0167-6105(90)90023-6

Matsumoto, M., Shiraishi, M., and Shirato, H. (1990). Aerodynamic instabilities of twin circular cylinders, *J. Wind Eng. Ind. Aerodyn.*, 33, 91-100. https://doi.org/10.1016/0167-6105(90)90024-7

Miyata, T., Yamada, H., Katsuchi, H., and Shinohara, K. (2000). Wind-tunnel-test study on WIV of parallel cables, *proceedings of 16th National Symposium on Wind Engineering*, 16, 489-494.

Mysa, R.C., Law, Y.Z., and Jaiman, R.K. (2017). Interaction dynamics of upstream vortex with vibrating tandem circular cylinder at subcritical Reynolds number, *J. Fluids Struct.*, 75, 27-44. https://doi.org/10.1016/j.jfluidstructs.2017.08.001

Price, S.J. (1975). Wake-induced flutter of power transmission conductors, *J. Sound Vib.*, 38(1), 125-147. https://doi.org/10.1016/s0022-460x(75)80023-x

Price, S.J. and Adballah, R. (1990). On the efficacy of mechanical damping and frequency detuning in alleviating wake-induced flutter of overhead power conductors, *J. Fluids Struct.*, 4(1), 1-34. https://doi.org/10.1016/0889-9746(90)90029-5

Qin, B., Alam, M.M., Ji, C., Liu, Y., and Xu, S. (2018). Flow-induced vibrations of two cylinders of different natural frequencies., *Ocean Eng.*, 155(1), 189–200. https://doi.org/10.1016/j.oceaneng.2018.02.048

Qin, B., Alam, M.M., and Zhou, Y. (2017). Two tandem cylinders of different diameters in cross-flow: flow-induced vibration., *J. Fluid Mech.*, 829, 621–658. https://doi.org/10.1017/jfm.2017.510

Qin, B., Alam, M.M., and Zhou, Y. (2019). Free vibrations of two tandem elastically mounted cylinders in crossflow. *J. Fluid Mech.*, 861, 349–381. https://doi.org/10.1017/jfm.2018.913

Ruscheweyh, H.P. (1983). Aeroelastic interference effects between slender structures. *J. Wind Eng. Ind. Aerodyn.*, 14, 129-140. https://doi.org/10.1016/0167-6105(83)90017-x

Sarkar, P.P., Jones, N.P., and Scanlan, R.H. (1994). Identification of Aeroelastic Parameters of Flexible Bridges, *J. Eng. Mech.*, 120(8), 1718-1742. https://doi.org/10.1061/(asce)0733-9399(1994)120:8(1718)

Scanlan, R.H. and Tomko, J.J. (1971). Airfoil and bridge deck flutter derivatives, *J. Eng. Mech. Div.*, 97(6), 1717-1737.

Shiraishi, M., Matsumoto, M., Shirato, H., Sagawa, N., and Yokota, T. (1984). On the aerodynamic instabilities of tandem circular cylinders, *Disaster Prevention Research Institute Annuals*, B-1, 27.

Shiraishi, M., Matsumoto, M., and Shirato, H. (1986). On aerodynamic instabilities of tandem structures, *J. Wind Eng. Ind. Aerodyn.*, 23, 437-447. https://doi.org/10.1016/0167-6105(86)90061-9

Simpson, A. (1971a). On the Flutter of a Smooth Circular Cylinder in a Wake. *Aeronautical Quarterly*, 22(1), 25-41. https://doi.org/10.1017/s000192590000562x

Simpson, A. (1971b). Wake Induced Flutter of Circular Cylinders: Mechanical Aspects. *Aeronautical Quarterly*, 22(2), 101-118. https://doi.org/10.1017/s0001925900005692

Simpson, A. and Flower, J.W. (1977). An improved mathematical model for the aerodynamic forces on tandem cylinders in motion with aeroelastic applications. *J. Sound Vib.*, 51(2), 183-217. https://doi.org/10.1016/s0022-460x(77)80032-1

Sumner, D., Price, S.J., and Païdoussis, M. P. (2000). Flow-pattern identification for two staggered circular cylinders in cross-flow, *J. Fluid Mech.*, 411, 263-303. https://doi.org/10.1017/s0022112099008137

Sumner, D. (2010). Two circular cylinders in cross-flow, *J. Fluids Struct.*, 26(6), 849-899. https://doi.org/10.1016/j.jfluidstructs.2010.07.001

Tokoro, S., Komatsu, H., Nakasu, M., Mizuguchi, K., and Kasuga, A. (2000). A study on wake-galloping employing full aeroelastic twin cable model, *J. Wind Eng. Ind. Aerodyn.*, 88(2), 247-261. https://doi.org/10.1016/s0167-6105(00)00052-0

Toriumi, R., Furuya, N., Takeguchi, M., Miyazaki, M., and Saito, Y. (1999). A study on wind-induced vibration of parallel suspenders observed at the Akashi-kaikyo bridge, *Proceedings of the 3rd International Symposium on Cable Dynamics*, 177-182.

Yagi, T., Arima, M., Araki, S., Ogawa, S., Kosugi, T., Zain, M.R.M., and Shirato, H. (2015). Investigation on wake-induced instabilities of parallel circular cylinders based on unsteady aerodynamic forces, *Proceedings of the 14th International Conference on Wind Engineering*, 1-12.

Yoshimura, T., Savage and M., and Tanaka, H. (1995). Wind induced vibrations of bridge stay-cables, *J. Wind Eng. Ind. Aerodyn.*, 54-55, 251-262. https://doi.org/10.1016/0167-6105(94)00045-f

Zdravkovich, M.M. (1977). Review of flow interference between two circular cylinders in various arrangements, *J. Fluids Eng.*, Transactions of the ASME, 618-633. https://doi.org/10.1115/1.3448871

Zdravkovich, M.M. and Pridden, D.L. (1977). Interference between two circular cylinders; series of unexpected discontinuities, *J. Ind. Aerodyn.*, 2(3), 255-270. https://doi.org/10.1016/0167-6105(77)90026-5

Zdravkovich, M.M. (1987). The effects of interference between circular cylinders in cross-flow, *J. Fluids Struct.*, 1(2), 239-261. https://doi.org/10.1016/s0889-9746(87)90355-0

Zhang, C., Kang, Z., Xiong, Y., Ai, S., and Ma, G., (2020). Experimental investigation on coupled cross-flow and in-line vortex-induced vibration responses of two staggered circular cylinders, *J. Eng. Maritime Environ.,* 235(1), 288-300 https://doi.org/10.1177/1475090220907473

Zhou, Y. and Alam, M. (2016). Wake of two interacting circular cylinders: A review, *Int. J. Heat Fluid Flow*, 62, 510-537. https://doi.org/10.1016/j.ijheatfluidflow.2016.08.008